High-Order Harmonic Generation of Heteronuclear Diatomic Molecules in Intense Ultrashort Laser Fields: An All-Electron TDDFT Study

JOHN HESLAR,[1,2] JUAN CARRERA,[1,2] DMITRY TELNOV,[3] SHIH-I CHU[1,2]

[1]*Department of Chemistry, University of Kansas, Lawrence, KS 66045, USA*

[2]*Center for Theoretical Sciences, Department of Physics, National Taiwan University, Taipei 106, Taiwan*

[3]*Department of Physics, St. Petersburg State University, 198504 St. Petersburg, Russia*

Received 29 April 2007; accepted 20 June 2007
Published online 6 August 2007 in Wiley InterScience (www.interscience.wiley.com).
DOI 10.1002/qua.21491

ABSTRACT: We present a time-dependent density functional theory (TDDFT), with proper asymptotic long-range potential, for nonperturbative treatment of multiphoton processes of homonuclear and heteronuclear diatomic molecules in intense ultrashort laser fields. A *time-dependent two-center generalized pseudospectral method* is presented for accurate and efficient treatment of the TDDFT equations in space and time. The procedure allows *nonuniform* and optimal spatial grid discretization of the Hamiltonian in prolate spheroidal coordinates and a split-operator scheme in the *energy representation* is used for the time propagation of the individual molecular spin-orbital. The theory is applied to a detailed *all-electron* study of multiphoton ionization (MPI) and high-order harmonic generation (HHG) processes of N_2 and CO molecules in intense laser pulses. The results reveal intriguing and substantially different nonlinear optical response behaviors for N_2 and CO, despite the fact that CO has only a very small permanent dipole moment. In particular, we found that the MPI rate for CO is higher than that of N_2. Furthermore, while laser excitation of the homonuclear N_2 molecule can generate only odd harmonics, both even and odd harmonics can be produced from the heteronuclear CO molecule. Int J Quantum Chem 107: 3159–3168, 2007

Key words: HHG; heteronuclear diatomic molecules; strong field; pseudospectral method; split operator

Correspondence to: S.-I. Chu; e-mail: sichu@ku.edu

Contract grant sponsors: US-NSF; Chemical Sciences, Geosciences and Biosciences, Division of the Office of Basic Energy Sciences, US Department of Energy; National Taiwan University.

Introduction

The study of atomic and molecular processes in intense ultrashort laser fields is a subject of much current interest in science and technology [1]. In particular, high-order harmonic generation (HHG) is one of the hottest topics in strong-field atomic and molecular physics today, which is closely related to the recent development of attosecond laser pulses [2–4] as well as the frequency comb technology [5–7]. To describe such strong-field processes using fully ab initio wave-function approach, it is necessary to solve the $(3n + 1)$ dimensional time-dependent Schrödinger equation (TDSE) in space and time, where n is the number of electrons. This is well beyond the capability of current supercomputer technology when $n > 2$. Even for the two-electron ($n = 2$) case, high-precision fully ab initio 6D study of the HHG of the He atoms was achieved only very recently [8]. For many-electron molecular ($n \geq 2$) systems, we have recently performed *self-interaction-free* time-dependent density functional theory (TDDFT) calculations for the nonperturbative treatment of multiphoton ionization (MPI) and HHG processes of homonuclear diatomic molecules H_2 [9], N_2 [10,11], O_2, and F_2 [11] in intense laser fields.

The motivation of this article is as follows. We extend the TDDFT, with proper long range potentials, to the study of multi-electron heteronuclear diatomic molecules (CO in particular) with an aim to explore the dynamical role and nonlinear response of individual electron spin orbital as well as the effect of asymmetry of the molecules to intense laser pulse fields, a subject of largely unexplored area of intense field AMO physics. In our previous studies of the MPI of homonuclear diatomic molecules N_2, O_2, and F_2, we found that the highest occupied molecular orbital (HOMO) is not necessary the dominant channel responding to the strong-field molecular ionization [11]. Furthermore the ac Stark shift of individual MO and the detailed molecular electronic structure need to be taken into account for a proper and quantitative treatment of the intense AMO processes. In the case of F_2, for example, while the HOMO is $1\pi_g$, the dominant MO channel to ionization in strong fields turns out to be the $3\sigma_g$ in intense laser fields [11]. Approximate models, such as ADK [12] and Keldysh [13] etc., which consider only the HOMO contributing to the molecular ionization and neglect the ac Stark effect, predicted the ionization suppression of F_2, in disagreement with the experimental observation [14,15]. In this article, we further explore the effect of the asymmetry of the molecules to MPI and HHG. We found that the heteronuclear diatomic molecules can contribute the generation of even harmonics, in addition to the odd harmonics seen in the atomic and homonuclear diatomic cases. Furthermore, we found that there is only one dominant (short-trajectory) rescattering event within each optical cycle. This is different from that seen in the atomic and homonuclear diatomic cases, where two dominant electron rescattering events, one from the short- and the other from the long-trajectory, occur within each optical cycle. Comparing the MPI and HHG behavior of CO with N_2, it reveals quite dramatic difference in their strong-field nonlinear responses, despite the fact that CO has only a very small (field-free) permanent dipole moment.

The organization of this article is as follows. First we briefly describe the TDDFT formalism for the general treatment of the multiphoton dynamics of heteronuclear and homonuclear diatomic molecular systems in the following section. Then we outline a generalized pseudospectral (GPS) method in the later section for *nonuniform* and optimal spatial discretization of the two-center molecular systems. In section "Time Dependent Generalized Pseudospectral Method For Numerical Solution of TDDFT Equation", we present a time-dependent GPS method for efficient and accurate solution of TDDFT equations in space and time. The method is then applied to the nonperturbative investigation of MPI of N_2 and CO in intense linearly polarized laser pulses in section "Multiphoton Ionization of N_2 and CO in Intense Laser Fields", and high harmonic generation of N_2 and CO in the second last section. This is followed by a conclusion in the last section.

Time-Dependent DFT for Homonuclear and Heteronuclear Diatomic Molecules

We first outline below the basic equations of TDDFT. The central theme of the TDDFT involves a set of time-dependent one-electron Schrödinger-like Kohn–Sham (KS) equations [16] for N-electron atomic or molecular systems (in atomic units),

$$i\frac{\partial}{\partial t}\psi_{i\sigma}(\boldsymbol{r},t) = \hat{H}(\boldsymbol{r},t)\psi_{i\sigma}(\boldsymbol{r},t) = \left[-\frac{1}{2}\nabla^2 + \upsilon_{\mathrm{eff},\sigma}(\boldsymbol{r},t)\right]\psi_{i\sigma}(\boldsymbol{r},t), \quad i = 1,2,\ldots,N_\sigma, \tag{1}$$

where $N_\sigma (= N_\uparrow \text{ or } N_\downarrow)$ is the total number of electrons for a given spin σ. The total number of electrons in the system is $N = \sum_\sigma N_\sigma$. The time-dependent effective potential $\upsilon_{\text{eff},\sigma}(\boldsymbol{r}, t)$ is a functional of the electron spin-densities $\rho_\sigma(\boldsymbol{r}, t)$.

The total electron density at time t is determined by the set of occupied single-electron Kohn–Sham spin-orbital wave functions $\psi_{i\sigma}$ as

$$\rho(\boldsymbol{r}, t) = \sum_\sigma \sum_{i=1}^{N_\sigma} \psi_{i\sigma}^* \psi_{i\sigma} = \sum_\sigma \sum_{i=1}^{N_\sigma} \rho_{i\sigma}(\boldsymbol{r}, t) = \rho_\uparrow(\boldsymbol{r}, t) + \rho_\downarrow(\boldsymbol{r}, t). \quad (2)$$

The effective potential $\upsilon_{\text{eff},\sigma}([\rho]; \boldsymbol{r}, t)$ in Eq. (1) can be written in the general form

$$\upsilon_{\text{eff},\sigma}([\rho]; \boldsymbol{r}, t) = \upsilon_{\text{H}}(\boldsymbol{r}, t) + \upsilon_{\text{ext}}(\boldsymbol{r}, t) + \upsilon_{\text{xc},\sigma}(\boldsymbol{r}, t), \quad (3)$$

where

$$\upsilon_{\text{H}}(\boldsymbol{r}, t) = \int \frac{\rho(\boldsymbol{r}', t)}{|\boldsymbol{r} - \boldsymbol{r}'|} d\boldsymbol{r}' \quad (4)$$

is the Hartree potential due to electron–electron Coulomb interaction, $\upsilon_{\text{ext}}(\boldsymbol{r}, t)$ is the "external" potential due to the interaction of the electron with the external laser field and the nuclei. In the case of CO or N_2 molecule in a linearly polarized external laser field, we have

$$\upsilon_{\text{ext}}(\boldsymbol{r}, t) = -\frac{Z_1}{|\boldsymbol{R}_1 - \boldsymbol{r}|} - \frac{Z_2}{|\boldsymbol{R}_2 - \boldsymbol{r}|} + (\boldsymbol{E}(t) \cdot \boldsymbol{r}) \sin \omega t. \quad (5)$$

where $\boldsymbol{r}$ is the electronic coordinate, $E(t)$ the electric field amplitude, $\boldsymbol{R}_1 = (0, 0, -a)$ and $\boldsymbol{R}_2 = (0, 0, b)$ are the coordinates of the two nuclei in Cartesian coordinates, and Z_1 and Z_2 are the electric charges of the two nuclei, respectively. The internuclear separation R is equal to $(a + b)$, where a and b are the positions of the two nuclei in the center-of-mass scheme. If the nuclear degree of freedom is not taken into account (frozen nuclei approximation), the total Hamiltonian will depend only upon R, as to be shown later. Finally, $\upsilon_{\text{xc},\sigma}(\boldsymbol{r}, t)$ is the time-dependent exchange-correlation (xc) potential. Since the exact form of $\upsilon_{\text{xc},\sigma}(\boldsymbol{r}, t)$ is unknown, the *adiabatic* approximation is often used [9, 17]

$$\upsilon_{\text{xc},\sigma}(\boldsymbol{r}, t) = \upsilon_{\text{xc},\sigma}[\rho_\sigma]|_{\rho_\sigma = \rho_\sigma(\boldsymbol{r}, t)}. \quad (6)$$

Note that if the conventional *explicit* xc energy functional forms taken from local spin density approximation (LSDA) or generalized gradient approximation (GGA) [18, 19] are used, the corresponding xc potential $\upsilon_{\text{xc},\sigma}(\boldsymbol{r}, t)$ will not possess the correct long-range asymptotic $(-1/r)$ behavior [20]. Here, we adopt the improved LB potential [21], $\upsilon_{\text{xc},\sigma}^{\text{LB}\alpha}$, which contains two empirical parameters α and β and has the following form, in the adiabatic approximation,

$$\upsilon_{\text{xc},\sigma}^{\text{LB}\alpha}(\boldsymbol{r}, t) = \alpha \upsilon_{\text{x},\sigma}^{\text{LSDA}}(\boldsymbol{r}, t) + \upsilon_{\text{c},\sigma}^{\text{LSDA}}(\boldsymbol{r}, t) - \frac{\beta x_\sigma^2(\boldsymbol{r}, t) \rho_\sigma^{1/3}(\boldsymbol{r}, t)}{1 + 3\beta x_\sigma(\boldsymbol{r}, t) \ln\{x_\sigma(\boldsymbol{r}, t) + [x_\sigma^2(\boldsymbol{r}, t) + 1]^{1/2}\}}. \quad (7)$$

Here, ρ_σ is the electron density with spin σ, and we use $\alpha = 1.19$ and $\beta = 0.01$ [10]. The first two terms in Eq. (7), $\upsilon_{\text{x},\sigma}^{\text{LSDA}}$ and $\upsilon_{\text{c},\sigma}^{\text{LSDA}}$ are the LSDA exchange and correlation potentials that do *not* have the correct asymptotic behavior. The last term in Eq. (7) is the nonlocal gradient correction with $x_\sigma(\boldsymbol{r}) = |\nabla \rho_\sigma(\boldsymbol{r})| / \rho_\sigma^{4/3}(\boldsymbol{r})$, which ensures the proper long-range asymptotic potential $\upsilon_{\text{xc},\sigma}^{\text{LB}\alpha} \to -1/r$ as $r \to \infty$. For the time-independent case, this exchange-correlation LBα potential has been found to be reliable for atomic and molecular DFT calculations.

Generalized Pseudospectral Discretization of Two-Center Heteronuclear and Homonuclear Diatomic Molecular Systems

In this section, we outline the generalized pseudospectral (GPS) method for nonuniform and optimal spatial discretization of two-center homonuclear and heteronuclear diatomic systems. We shall use the following prolate spheroidal coordinates (ξ, η, φ) [22], $1 < \xi < \infty$, $-1 < \eta < 1$, $0 < \varphi < 2\pi$, for the description of the system

$$x = \frac{R}{2} \sqrt{(\xi^2 - 1)(1 - \eta^2)} \cos \varphi, \quad (8)$$

$$y = \frac{R}{2} \sqrt{(\xi^2 - 1)(1 - \eta^2)} \sin \varphi, \quad (9)$$

$$z = \frac{R}{2} \xi \eta, \quad (10)$$

where $R = (a + b)$ is the internuclear separation of the diatomic molecule.

Because of the axial symmetry with respect to the z-axis, the projection M of the angular momentum on the z-axis is conserved, therefore the wave function $\Psi(\xi,\eta,\varphi)$ takes the form

$$\Psi(\xi,\eta,\varphi)=\Phi(\xi,\eta)e^{iM\varphi},\quad (M=0,\pm1,\pm2,\ldots). \tag{11}$$

The field-free Hamiltonian of Eq. (1) for CO and N_2 molecules, in atomic units, can be written as

$$\hat{H}_0(\boldsymbol{r})=-\frac{1}{2}\nabla^2-\frac{Z_1}{|\boldsymbol{R}_1-\boldsymbol{r}|}-\frac{Z_2}{|\boldsymbol{R}_2-\boldsymbol{r}|}+\upsilon_{\mathrm{H}}(\boldsymbol{r})+\upsilon_{\mathrm{xc},\sigma}(\boldsymbol{r}). \tag{12}$$

Equation (12) can be recast into prolate spheroidal coordinates, which has the following form:

$$\hat{H}_0(\xi,\eta)=-\frac{2}{R^2}\frac{1}{(\xi^2-\eta^2)}\left[\frac{\partial}{\partial\xi}(\xi^2-1)\frac{\partial}{\partial\xi}+\frac{\partial}{\partial\eta}(1-\eta^2)\frac{\partial}{\partial\eta}-\frac{M^2(\xi^2-\eta^2)}{(\xi^2-1)(1-\eta^2)}\right]$$
$$-\frac{Z_1(\xi-\eta)}{a(\xi^2-\eta^2)}-\frac{Z_2(\xi+\eta)}{a(\xi^2-\eta^2)}+\upsilon_{\mathrm{H}}(\xi,\eta)+\upsilon_{\mathrm{xc},\sigma}(\xi,\eta), \tag{13}$$

where angular momentum $M=0$ for σ states, and $M=1$ for π states.

Now we consider *nonuniform* and optimal grid discretization of the spatial coordinates by means of the two-center *generalized pseudospectral* (GPS) technique. We shall use the following mapping transformations for the coordinates ξ and η:

$$\eta(y)=y,\quad -1\le y\le 1, \tag{14}$$

$$\xi(x)=1+L\frac{1+x}{1-x},\quad -1\le x\le 1, \tag{15}$$

L being the mapping parameter. The variables x and y are discretized using the Gauss–Legendre abscissas x_i and y_j as the collocation points. The sets of collocation points are described in previous works [10, 22, 23]. The Gauss–Legendre quadrature can be written as follows:

$$\int d^3r\Phi^2=2\pi a^3\sum_{i=1}^{N_\xi}\sum_{j=1}^{N_\eta}\phi_{ij}^2, \tag{16}$$

where N_ξ and N_η are the numbers of collocation points x_i and y_j, respectively. The values of ϕ_{ij} are related to the function Φ at the collocation points x_i and y_j,

$$\Phi(\xi(x_i),\eta(y_j))=\sqrt{\frac{(1-x_i^2)(1-y_j^2)}{\xi_i'\eta_j'(\xi_i^2-\eta_j^2)}}P'_{N_\xi}(x_i)P'_{N_\eta}(y_j)\phi_{ij}. \tag{17}$$

In Eq. (17), the primes denote the derivatives of the functions with respect to their arguments.

The discretized electronic Hamiltonian Eq. (13) is a matrix of order $N_\xi N_\eta\times N_\xi N_\eta$ which acts on the vector $\{\phi_{ij}\}$, the matrix elements being

$$H_{ij;i'j'}=\frac{2}{R^2}\left[\delta_{jj'}\frac{\eta_j'}{(1-y_j^2)}\sum_{k=1}^{N_\xi}\frac{1}{\xi_k'}\frac{(\xi_k^2-1)}{(1-x_k^2)}D_{ki}^{(x)}D_{ki'}^{(x)}+\delta_{ii'}\frac{\xi_i'}{(1-x_i^2)}\sum_{k=1}^{N_\eta}\frac{1}{\eta_k'}\frac{(1-\eta_k^2)}{(1-y_k^2)}D_{kj}^{(y)}D_{kj'}^{(y)}\right]$$
$$\times\sqrt{\frac{(1-x_i^2)(1-y_j^2)}{\xi_i'\eta_j'(\xi_i^2-\eta_j^2)}}\sqrt{\frac{(1-x_{i'}^2)(1-y_{j'}^2)}{\xi_{i'}'\eta_{j'}'(\xi_{i'}^2-\eta_{j'}^2)}}+\delta_{ii'}\delta_{jj'}\left[\frac{1}{2a^2}\frac{M^2(\xi_i^2-\eta_j^2)}{(1-\eta_j^2)(\xi_i^2-1)}-\frac{Z_1(\xi_i-\eta_j)}{a(\xi_i^2-\eta_j^2)}\right.$$
$$\left.-\frac{Z_2(\xi_i+\eta_j)}{a(\xi_i^2-\eta_j^2)}+\upsilon_{\mathrm{H}}(\xi_i,\eta_j)+\upsilon_{\mathrm{xc},\sigma}(\xi_i,\eta_j)\right]. \tag{18}$$

The first derivative matrices $D_{ii}^{(x)}$, $D_{jj}^{(y)}$ have simple analytical expressions in the pseudospectral method; a detailed construction is given elsewhere [22]. Equations (16)–(18) are the main results of the current Gauss–Legendre pseudospectral discretization in the prolate spheroidal coordinates, which are different from our previous calculations [9–11] of homonuclear diatomic systems.

TABLE I

Comparison of the field-free molecular orbital energy levels of CO and N_2, calculated with the LB_α potential, and the experimental ionization potentials (in a.u.).

Orbital	Expt.[a]	LB_α
CO		
1σ	19.9367	19.6142
2σ	10.8742	10.6556
3σ	1.3964	1.2549
4σ	0.7239	0.7071
1π	0.6247	0.6276
5σ	0.5144	0.5086
N_2		
$1\sigma_g$	15.0492	14.7962
$1\sigma_u$	15.0492	14.7950
$2\sigma_g$	1.3708	1.2162
$2\sigma_u$	0.6883	0.6786
$1\pi_u$	0.6233	0.6199
$3\sigma_g$	0.5726	0.5682

[a]Experimental ionization potential for CO and N_2 are calculated using Ref. 25 and Refs. 26–28, respectively.

The ground-state electronic configurations is $1\sigma_g^2 1\sigma_u^2 2\sigma_g^2 2\sigma_u^2 1\pi_u^4 3\sigma_g^2$ for N_2 and $1\sigma^2 2\sigma^2 3\sigma^2 4\sigma^2 1\pi^4 5\sigma^2$ for CO, respectively. N_2 and CO are isoelectronic molecules, both having 14 electrons and triple bonds. Since the CO molecule has unequal nuclear charges, its ground electronic state possesses a permanent dipole moment, calculated here to be 0.149 Debye. The corresponding experimental value is 0.112 Debye [24]. Furthermore, there is no concept of gerade and ungerade orbitals for CO (or any other heteronuclear diatomic molecule) since the inversion symmetry of the potential is broken. Table I lists the MO energies calculated with the LBα potential, using 50 grid points in ξ and 30 grid points in η. The agreement of the calculated valence MO energies with the experimental data is well within 0.01 a.u.

Time-Dependent Generalized Pseudospectral Method for Numerical Solution of TDDFT Equation

In this section, we outline the time-dependent generalized pseudospectral (TDGPS) procedure for the solution of the set of time-dependent equations, Eq. (1), for the CO and N_2 molecules. The advantage of this method is that it allows nonuniform and optimal spatial grid discretization (denser mesh near each nucleus and sparser mesh at larger electron-nucleus separations). This improves greatly both the accuracy and the efficiency of the electronic structure and time-dependent calculations. The commonly used procedures for the time propagation of the Schrödinger or TDDFT equation employ *equal-spacing* spatial-grid discretization [29]. For processes such as HHG, accurate time-dependent wave functions are required to achieve convergence since the intensity of various harmonic peaks can span a range of many orders of magnitude. High precision accuracy is generally more difficult to achieve by the equal-spacing spatial-grid-discretization time-dependent techniques. The TDGPS method consist of the following two basic steps. (i) A two-center GPS technique [22] is used for optimal grid discretization of the pseudoradial (ξ) and pseudoangular (η) coordinates. The number of grid points required is generally considerably smaller than those used by the equal-spacing discretization methods. Yet higher accuracy in wave functions and therefore HHG spectra can be achieved, since the physically more important short-range regime is treated accurately by this method. The TDGPS method also has been recently applied successfully to the non-Hermitian Floquet studies of the hydrogen molecular ion H_2^+ in strong fields [22]. (ii) A split-operator technique in the *energy* representation is introduced for efficient time propagation of the wave functions. In this work, we extend this procedure to the numerical solution of the two-centered systems in the time-dependent equations.

Consider now the solution of the TDDFT equation, Eq. (1), recasted into the following form:

$$i\frac{\partial}{\partial t}\psi_{i\sigma}(\boldsymbol{r},t) = \hat{H}(r,t)\psi_{i\sigma}(\boldsymbol{r},t) = [\hat{H}_0(\boldsymbol{r}) + \hat{V}(\boldsymbol{r},t)] \times \psi_{i\sigma}(\boldsymbol{r},t), \quad i = 1,2,\ldots,N_\sigma \quad (19)$$

where $\hat{H}_0$ is the time-independent Hamiltonian whose matrix elements are given in Eq. (18), and $\hat{V}(\boldsymbol{r},t)$ includes the electron-laser field interaction and other residual time-dependent terms in $\upsilon_{\mathrm{eff},\sigma}([\rho];\boldsymbol{r},t)$:

$$\hat{V}(\boldsymbol{r},t) = (\boldsymbol{E}(t)\cdot\boldsymbol{r})\sin\omega t + (\upsilon_{\mathrm{H}}(\boldsymbol{r},t) - \upsilon_{\mathrm{H}}(\boldsymbol{r},0)) + (\upsilon_{\mathrm{xc},\sigma}(\boldsymbol{r},t) - \upsilon_{\mathrm{xc},\sigma}(\boldsymbol{r},0)). \quad (20)$$

Here $\boldsymbol{E}(t)$ is the electric field parallel to the internuclear ($\hat{\boldsymbol{z}}$) axis, and $E(t) = Ff(t)$, where $f(t)$ is the envelope function of the laser pulse. We shall

extend the second-order split-operator technique in prolate spheroidal coordinates and in the *energy* representation [23,30] for the propagation of individual spin-orbital

$$\psi_{i\sigma}(\boldsymbol{r}, t+\triangle t) \simeq e^{-i\hat{V}(\boldsymbol{r},t)\triangle t/2} e^{-i\hat{H}_0(\boldsymbol{r})\triangle t} e^{-i\hat{V}(\boldsymbol{r},t)\triangle t/2} \psi_{i\sigma}(\boldsymbol{r}, t) + O(\triangle t^3). \quad (21)$$

Note that such an expression is different from the conventional split-operator techniques [31, 32], where $\hat{H}_0$ is usually chosen to be the kinetic-energy operator and $\hat{V}$ the remaining Hamiltonian depending on the spatial coordinates only. The use of the *energy* representation in Eq. (21) allows the explicit *elimination* of the undesirable fast-oscillating *high-energy* components and speeds up considerably the time propagation [9, 23, 30]. After the time-dependent single electron wave functions $\{\psi_{i\sigma}\}$ are obtained, the total electron density $\rho(\boldsymbol{r}, t)$ can be determined.

The time-dependent induced dipole moment can now be calculated as

$$d(t) = \int z\rho(\boldsymbol{r}, t) d\boldsymbol{r} = \sum_{i\sigma} d_{i\sigma}(t), \quad (22)$$

where

$$d_{i\sigma}(t) = n_{i\sigma} \langle \psi_{i\sigma}(\boldsymbol{r}, t) \, |z| \psi_{i\sigma}(\boldsymbol{r}, t) \rangle, \quad (23)$$

is the induced dipole moment of the $i\sigma$-th spin orbital, and $n_{i\sigma}$ is its electron occupation number. The power spectrum of the HHG is then acquired by taking the Fourier transform of the total time-dependent induced dipole moment $d(t)$:

$$P(\omega) = \frac{4\omega^4}{3c^3} \left| \frac{1}{t_f - t_i} \int_{t_i}^{t_f} d(t) e^{-i\omega t} dt \right|^2. \quad (24)$$

Here c is the speed of light, and $P(\omega)$ has the meaning of the energy emitted per unit time at the particular photon frequency ω.

Multiphoton Ionization of N_2 and CO in Intense Laser Fields

Once the time-dependent wave functions and the time-dependent electron densities are obtained, we can calculate the time-dependent (multiphoton) ionization probability of an individual spin-orbital according to

$$P_{i,\sigma} = 1 - N_{i,\sigma}(t), \quad (25)$$

where

$$N_{i,\sigma}(t) = \langle \psi_{i,\sigma}(t) | \psi_{i,\sigma}(t) \rangle, \quad (26)$$

is the time-dependent population (survival probability) of the $i\sigma$-th spin-orbital.

Figure 1 presents the time-dependent population of individual spin orbital, as defined in Eq. (26). The slope of the decay of the electron population in time determines the ionization rate. The laser (electric) field is assumed to be parallel to the internuclear axis, and the internuclear distance for the CO ($R_e = 2.132\, a_0$) and N_2 ($R_e = 2.072\, a_0$) molecules is fixed at its equilibrium distance R_e. Results for two laser intensities (5×10^{13} and 1×10^{14} W/cm^2) and a wavelength of 800 nm, 20-optical-cycle laser pulse are shown for CO and N_2. The orbital structure and ionization potentials of the two molecules under consideration are close to each other. That is why one can expect similar behavior in the laser field with the same wavelength and intensity. The multiphoton ionization in the laser field is dominated by HOMO, that is $3\sigma_g$ in N_2 and 5σ in CO. As one can see from Figures 1(a) and (c), at lower intensity 5×10^{13} W/cm^2, the HOMO survival probabilities of N_2 and CO are close to each other. However, at higher intensities, the difference becomes more pronounced, at the intensity 1×10^{14} W/cm^2, the ionization probability of CO is much larger than that of N_2 [Figs. 1(b) and (d)]. The explanation of the phenomenon can be as follows. In intense low-frequency laser fields, the multiphoton ionization occurs mainly in the tunneling regime. In this picture, the ionization takes place in the DC field with slowly varying amplitude from zero to its peak value. The width of the potential barrier depends on the field strength; the stronger the field, the narrower the barrier. Thus the ionization occurs mainly at the peak values of the field strength. The probability of the tunneling ionization is very sensitive with respect to the HOMO energy. However, in the external field this energy is changed due to the Stark shift. The nitrogen molecule is symmetric with respect to inversion, that is why the Stark shift in the DC field is quadratic in the field strength and its value is quite small. On the contrary, the carbon monoxide molecule has a permanent dipole moment, and the DC Stark shift is linear in the field

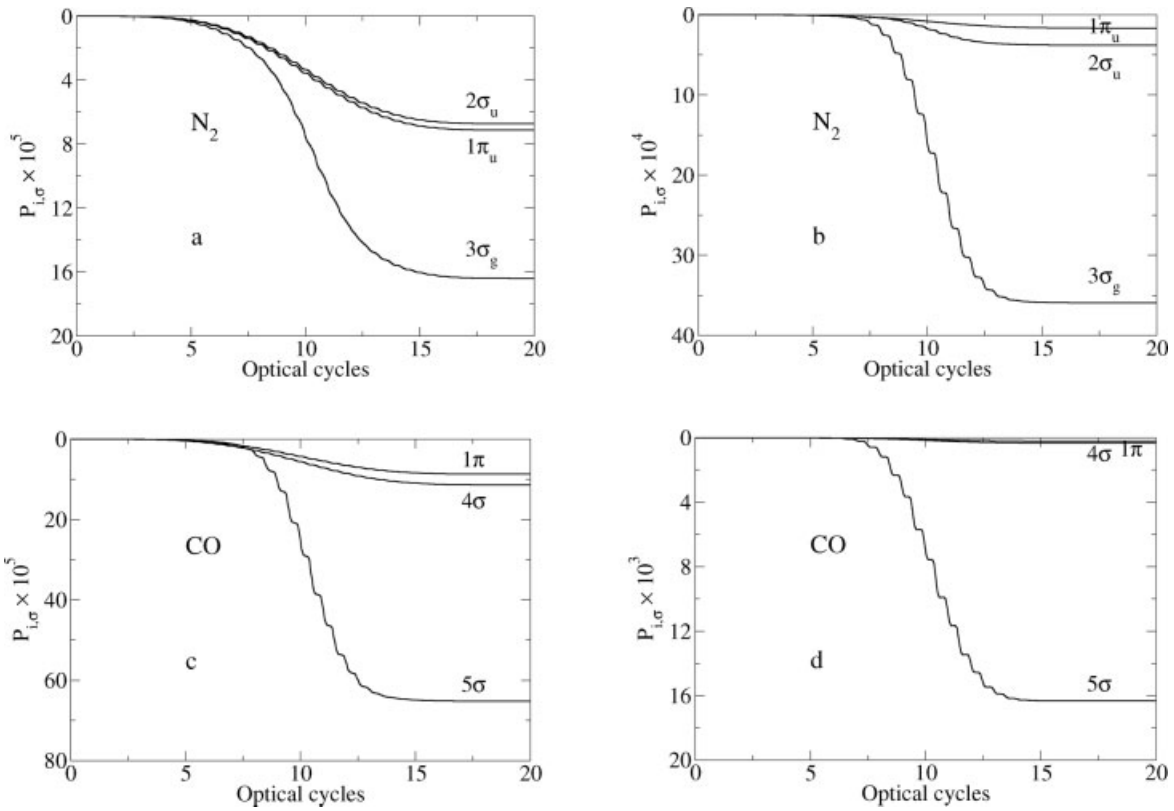

FIGURE 1. The time-dependent population of electrons in different spin orbital's of CO and N_2 in 800 nm, $\sin^2$ pulse laser field, with 20 optical cycles in pulse duration. N_2 molecule (a) 5×10^{13} W/cm^3, (b) 1×10^{14} W/cm^2, CO molecule (c) 5×10^{13} W/cm^2, (d) 1×10^{14} W/cm^2.

strength; at the peak values of the field, the HOMO energy can differ significantly from its unperturbed value. We have performed the self-consistent DFT calculations of N_2 and CO in the DC electric field parallel to the molecular axis to see how large the Stark shift can change the ionization potential of the molecule. On Table II we show the HOMO energies computed at the field strength 0.7549×10^{-2} a.u., which corresponds to the intensity 2×10^{12} W/cm^2. As one can see, even in the field as weak as 2×10^{12} W/cm^2, the shift of the HOMO energy in CO molecule is large. The shift depends on the direction of the external field with respect to the position of the carbon and oxygen nuclei. In one direction the energy level becomes higher, and in the other direction it becomes lower than the unperturbed level. Decrease of the binding energy will result in the enhanced ionization. In intense low-frequency laser fields, this effect can be responsible for the enhancement of ionization of CO molecule as compared with N_2.

TABLE II

HOMO energies of N_2 and CO molecules in DC electric field (positive field direction is from C to O).

Electric field (a.u.)	N_2 HOMO energy (a.u.)	CO HOMO energy (a.u.)
0	−0.5682	−0.5086
0.7549×10^{-2}	−0.5681	−0.5149
-0.7549×10^{-2}	−0.5681	−0.5026

High-Order Harmonic Generation of Heteronuclear and Homonuclear Diatomic Molecules in Intense Laser Fields

In Figures 2 and 3 we present the high-order harmonic generation (HHG) power spectra [HHG power, Eq. (24)] for the laser field intensities 5×10^{13}, and 1×10^{14} W/cm^2. An important difference

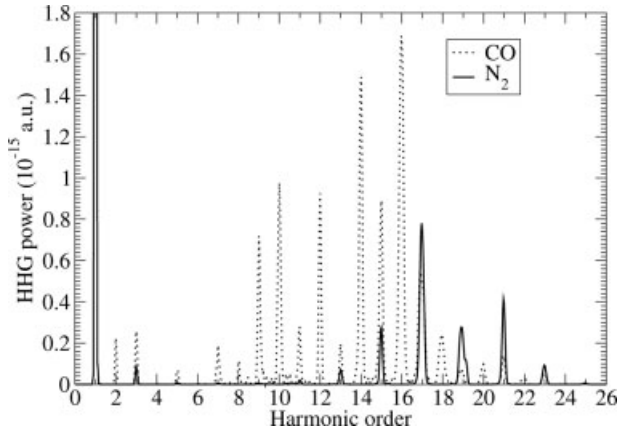

FIGURE 2. Comparison of the HHG power spectra of CO and N_2, in 800 nm, 5×10^{13} W/cm^2 sin^2 pulse laser field.

between the N_2 and CO spectra is that the latter contain even as well as odd harmonics. Generation of even harmonics is forbidden in systems with inversion symmetry, such as atoms and homonuclear diatomic molecules. This selection rule does not apply to the heteronuclear molecules with no inversion center (CO). From Figures 2 and 3, one can see that in general HHG is more efficient in CO than in N_2. However, for higher harmonics (17 and above) the N_2 spectra become dominant at the same laser intensity. As the laser intensity increases, the maximum in the power spectra is shifted towards higher harmonics.

To investigate the detailed spectral and temporal structure of HHG for homonuclear and

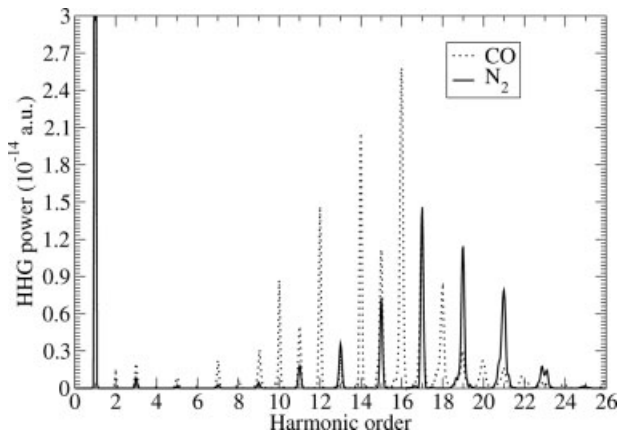

FIGURE 3. Comparison of the HHG power spectra of CO and N_2, in 800 nm, 1×10^{14} W/cm^2 sin^2 pulse laser field.

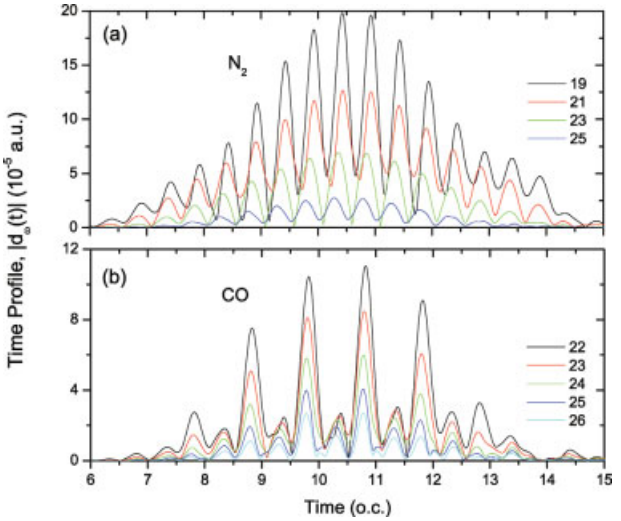

FIGURE 4. Time profiles for (a) N_2 and (b) CO. Laser intensity used is 5×10^{13} W/cm^2, wavelength used is 800 nm, with 20 optical cycles in pulse duration. [Color figure can be viewed in the online issue, which is available at www.interscience.wiley.com.]

heteronuclear systems, we perform the time-frequency analysis by means of the wavelet transform of the total induced dipole moment $d(t)$ [9,33],

$$d_\omega(t) = \int d(t)\sqrt{\frac{\omega}{\tau}}\exp\left[i\omega(t-t_0)\right] \times \exp\left[-(\omega(t-t_0))^2/2\tau^2\right]dt. \quad (27)$$

The parameter $\tau = 15$ is chosen to perform the wavelet transformation in the following study. The peak emission times, t_e, represent the instance when the maxima of the dipole time profile occur, and semiclassically are interpreted as the electron-ion recollision times [33]. For the case of the N_2 molecule, the time profiles of the 19th to 25th harmonic orders are shown in Figure 4(a). There are two emissions occurring at each optical cycle, and the most prominent bursts take place at the center of the laser field envelope. The time profiles of the superimposed harmonics are rather uniform among themselves implicating that the harmonics are partially synchronized. More importantly for the CO molecule, a distinct feature possibly characteristic of all heteronuclear diatomic systems is observed in Figure 4(b) for the harmonic orders 22nd to 26th. The number of dominant emissions per optical cycle is now limited to only one. This finding is in contrast with results normally obtained in the HHG for atoms

and homogeneous molecules in which two bursts per optical cycle are observed. The spectral profiles are as uniform as those obtained for N_2, though the CO harmonics appear to be more synchronized than those of N_2.

Conclusion

In this article, we present a detailed comparison of the very high-order nonlinear optical response of the homonuclear N_2 and heteronuclear CO diatomic molecules in intense ultrashort laser fields by means of a TDDFT with correct asymptotic long-range $(-1/r)$ potential to ensure individual spin-orbital has the proper ionization potential. We consider only the case that the molecular axis is aligned with the laser beam direction. This is justified based on the recent experimental development of the laser molecular alignment techniques [34–37]. We found that although CO has only a very small permanent dipole moment, qualitatively different nonlinear optical responses are predicted for CO and N_2. First, the MPI rate for the heteronuclear diatomic CO molecules is larger than that for the N_2 homonuclear diatomic molecules. Second, while the laser excitation of the N_2 molecules can generate only odd harmonics, both even and odd harmonics can be produced for the CO case. To our knowledge, this is the first *all-electron* TDDFT study of the generation of even harmonics for the heteronuclear diatomic molecules. In this connection, we note that the even-order harmonics were also predicted in an earlier study of the HHG of a one-dimensional model HD with unequal nuclear mass [38]. In this model, even-order harmonics can be produced only by means of the breakdown of the Born-Oppenheimer approximation. However, in our ab initio 3D study of CO with unequal nuclear mass and charge, even-order harmonics can still be produced when the internuclear separation is fixed. Third, from our wavelet time-frequency analysis, we found that there are two dominant rescattering (and harmonic emission) events within each optical cycle for the N_2 molecules, whereas there is only one dominant rescattering event for the CO molecules. Much remains to be explored in this fascinating and largely unexplored area of strong-field molecular physics. Finally, the nuclear degree of freedom has not been taken into account so far. This is justified for ultrashort laser pulse excitation. Research in this direction will be pursued in the future.

References

1. Brabec, T.; Krausz, F. Rev Mod Phys 2000, 72, 545.
2. Baltuška, A.; Udem, Th.; Uiberacker, M.; Hentschel, M.; Goulielmakis, E.; Gohle, Ch.; Holzwarth, R.; Yakovlev, V. S.; Scrinzi, A.; Hänsch, T. W.; Krausz, F. Nature (London) 2003, 421, 611.
3. Udem, Th.; Holzwarth, R.; Hänsch, T. W. Nature (London) 2002, 416, 233.
4. Hentschel, M.; Kienberger, R.; Spielmann, Ch.; Reider, G. A.; Milosevic, N.; Brabec, T.; Corkum, P.; Heinzmann, U.; Drescher, M.; Krausz, F. Nature (London) 2001, 414, 509.
5. Gohle, Ch.; Udem, Th.; Herrmann, M.; Rauschenberger, J.; Holzwarth, R.; Schuessler, H. A.; Krausz, F.; Hänsch, T. W. Nature (London) 2005, 436, 234.
6. Jones, R. J.; Moll, K. D.; Thorpe, M. J.; Ye, J. Phys Rev Lett 2005, 94, 193201.
7. Carrera, J.; Chu, S. I. Phys Rev Lett (submitted).
8. Guan, X. X.; Tong, X. M.; Chu, S. I. Phys Rev A 2006, 73, 023403.
9. Chu, X.; Chu, S. I. Phys Rev A 2001. 63, 023411.
10. Chu, X.; Chu, S. I. Phys Rev A 2001, 64, 063404.
11. Chu, X.; Chu, S. I. Phys Rev A 2004, 70, 061402(R).
12. Tong, X. M.; Zhao, Z. X.; Lin, C. D. Phys Rev A 2002, 66, 033402.
13. Muth-Bohm, J.; Becker, A.; Faisal, F. H. M. Phys Rev Lett 2000, 85, 2280.
14. DeWitt, M. J.; Wells, E.; Jones, R. R. Phys Rev Lett 2001, 87, 153001.
15. Wells, E.; DeWitt, M. J.; Jones, R. R. Phys Rev A 2002, 66, 013409.
16. Kohn, W.; Sham, L. J. Phys Rev 1965, 140, A1133.
17. Ullrich, C. A.; Gossmann, U. J.; Gross, E. K. U. Phys Rev Lett 1995, 74, 872.
18. Parr, R. G.; Yang, W. T. Density-Functional Theory of Atoms and Molecules; Oxford University Press: New York, 1989.
19. Dreizler, R. M.; Gross, E. K. U. Density Functional Theory, An Approach to Quantum Many-Body Probelm; Springer: Berlin, 1990.
20. Tong, X. M.; Chu, S. I. Phys Rev A 1997, 55, 3406.
21. Schipper, P. R. T.; Gritsenko, O. V.; van Gisbergen, S. J. A.; Baerends, E. J. J Chem Phys 2000, 112, 1344.
22. Telnov, D. A.; Chu, S. I. Phys Rev A 2005, 71, 013408.
23. Chu, X.; Chu, S. I. Phys Rev A 2000, 63, 013414.
24. Nelson, R. D., Jr.; Lide, D. R.; Maryott, A. A. National Standard Reference Data Series Natl. Bur. Stand. (U.S.) Circ. No. 10; US GPO: Washington, DC, 1967, p 1.
25. Siegbahn, K. J. Electron Spectrosc Relat Phenom 1974, 5, 3.
26. Johansson, G.; Hedman, J.; Berndtsson, A.; Klasson, M.; Nilsson, R. J Electron Spectrosc Relat Phenom 1973, 2, 295.
27. Hamnett, H.; Stoll, W.; Brion, C. E. J Electron Spectrosc Relat Phenom 1976, 8, 367.

28. Turner, D. W.; Baker, C.; Baker, A. D.; Brundle, C. R. Molecular Photoelectron Spectroscopy; Wiley-Interscience: London, 1970.
29. Kulander, K., Ed. Comput Phys Commun 1991, 63, 1.
30. Tong, X. M.; Chu, S. I. Chem Phys 1997, 217, 119.
31. Hermann, M. R.; Fleck, J. A., Jr. Phys Rev A 1988, 38, 6000.
32. Jiang, T. F.; Chu, S. I. Phys Rev A 1992, 46, 7322.
33. Tong, X. M.; Chu, S. I. Phys Rev A 61, 2000, 021802(R).
34. Leibscher, M.; Averbukh, I. S.; Rabitz, H. Phys Rev A 2004, 69, 013402.013402
35. Stapelfeldt, H.; Seideman, T. Rev Mod Phys 2003, 75, 543.
36. Pinkham, D.; Jones, R. R. Phys Rev A 2005, 72, 023418.
37. Pinkham, D.; Mooney, K. E.; Jones, R. R. Phys Rev A 2007, 75, 013422.
38. Kreibich, T.; Lein, M.; Engel, V.; Gross, E. K. U. Phys Rev Lett 2001, 87, 103901.